Hydroxyapatite implants with designed internal architecture

T.-M. G. CHU[1], J. W. HALLORAN[2], S. J. HOLLISTER[1], S. E. FEINBERG[3]
[1]Department of Biomedical Engineering, University of Michigan, Ann Arbor, MI 48109, USA
[2]Department of Materials Science and Engineering, University of Michigan, Ann Arbor, MI 48109, USA
[3]Department of Surgery, University of Michigan, Ann Arbor, MI 48109, USA
E-mail: ctmin@engin.umich.edu

Porous hydroxyapatite (HA) has been used as a bone graft material in the clinics for decades. Traditionally, the pores in these HAs are either obtained from the coralline exoskeletal patterns or from the embedded organic particles in the starting HA powder. Both processes offer very limited control on the pore structure. A new method for manufacturing porous HA with designed pore channels has been developed. This method is essentially a lost-mold technique with negative molds made with Stereolithography and a highly loaded curable HA suspension as the ceramic carrier. Implants with designed channels and connection patterns were first generated from a Computer-Aided-Design (CAD) software and Computer Tomography (CT) data. The negative images of the designs were used to build the molds on a stereolithography apparatus with epoxy resins. A 40 vol% HA suspension in propoxylated neopentyl glycol diacrylate (PNPGDA) and iso-bornyl acrylate (IBA) was formulated. HA suspension was cast into the epoxy molds and cured into solid at 85 °C. The molds and acrylate binders were removed by pyrolysis, followed by HA green body sintering. With this method, implants with six different channel designs were built successfully and the designed channels were reproduced in the sintered HA implants. The channels created in the sintered HA implants were between 366 μm and 968 μm in diameter with standard deviations of 50 μm or less. The porosity created by the channels were between 26% and 52%. The results show that HA implants with designed connection pattern and well controled channel size can be built with the technique developed in this study.

1. Introduction

Hydroxyapatite (HA) is a calcium phosphate that makes up the majority of the inorganic component of human bones and teeth. HA prepared in porous blocks or granules has been studied extensively as a bone graft material [1, 2]. The compatibility of these porous HA implants with bone tissues has been demonstrated in several researches [3–7]. Several manufacturing techniques have been developed for making these porous HAs. Two methods are most widely used. The first method was developed by Roy and Linnehan by using a hydrothermal exchange process to derive porous HA from reef building corals [8]. The calcium carbonate in the coral exoskeleton is converted into HA with the structural pattern of the coral exoskeleton preserved. The connecting channels in the final HA implants are provided by the natural coral exoskeleton architecture. Implants of this type have been studied extensively [3–5, 7, 9, 10]. A second method of making porous HA involves embedding organic particles, such as polyvinyl butyral [11, 12], naphthalene [13], and acrylic beads [14] in HA powder. HA powder is dry-pressed along with the organic particles. At high temperature, the organic particles are pyrolyzed, leaving pores in the size range of the original particle. The green body is then sintered into ceramics. In both processes, the control over the internal porous structure of the implants is very minimal. Undesirable isolated pores and blind ends are common in implants manufactured with the organic particle technique [2]. The coralline HA only contains the porous structure provided by the exoskeleton pattern of the harvested coral. The hydrothermal exchange process does not offer any control over the porous structure.

In this research, we have explored a new technique of manufacturing porous HA implants with designed channel pattern. This process is essentially a lost-mold shape forming process involving the use of StereoLithography (SL) and a highly loaded ''reactive ceramic suspension''. SL is a technique capable of taking the 3D computer scanning image or the computer design of an object and constructs a three-dimensional representation of the object from epoxy resin [15]. Several

researchers have demonstrated the versatility of this technology in making complicate-geometry objects like surgical models [16–19]. ''Reactive ceramic suspension'' refers to a ceramic suspension with ceramic powder dispersed in a reactive medium that can be polymerized or cured by heat or radiation. Ceramic suspensions like these have been used to make net-shape ceramics. Venkataswamy *et al.* [20] dispersed ceramic powders in acrylate monomers, which were later injected into molds and cured by heat. The cured suspension was removed from the mold and the acrylate binder was pyrolyzed, followed by sintering of the green bodies into ceramics. Similarly, Janney [21] dispersed ceramic powders in trimethylol propane triacrylate and hexanediol diacrylates. The suspensions were polymerized by a free-radical thermal initiator. The binder-removal and sintering process were similar to what was described above. Young *et al.* [22] developed an aqueous ceramic suspension by dispersing alumina powder in acrylamide (AM) and *N, N′*-methylenebisacrylamide (MBAM). Ceramic objects with complicated shapes were made with this aqueous ceramic suspension.

In this investigation, a highly loaded HA-acrylate suspension was developed and characterized. Epoxy molds with designed interconnected beams and channels were made with an SL apparatus (SLA-25O, 3D Systems, Valencia, CA). HA suspension was cast into the molds and was thermally cured. The epoxy molds and the interconnected beams were removed by pyrolysis to create the channel space in the implants. The acrylic binders in the cured HA suspensions were removed at the same time with the epoxy molds. Upon sintering, the pore channels left by the epoxy beams were preserved and the hydroxyapatite green body was densified to solid beams. The channel size, wall size, and the total porosity of the final implants were characterized. The overall process is illustrated in Fig. 1.

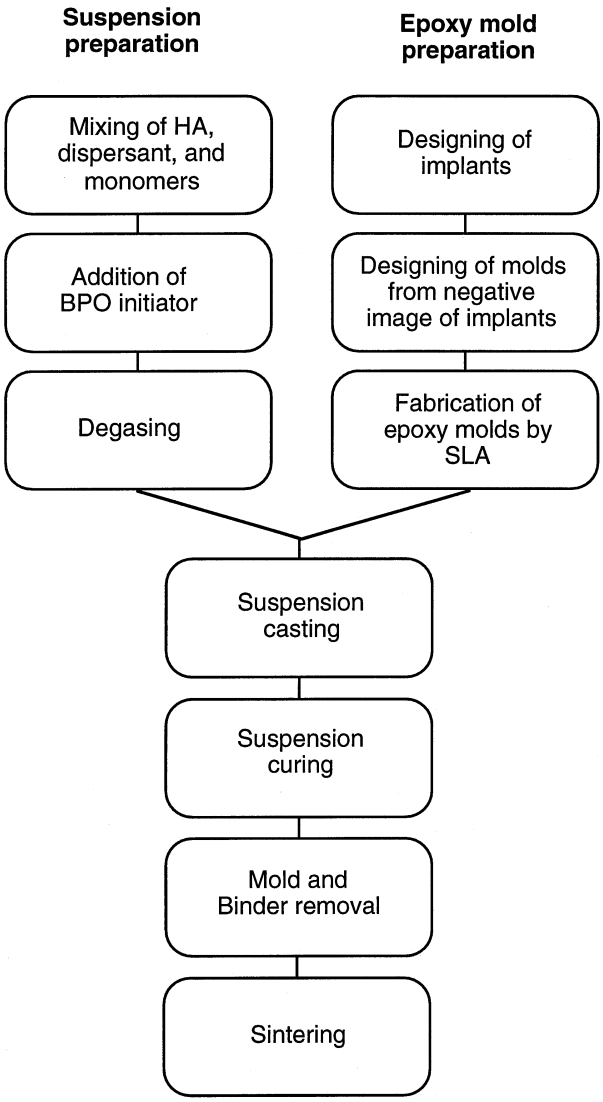

Figure 1 Flow chart of HA implant manufacturing process.

2. Experimental Procedures

2.1. Powder characterization

Commercial hydroxapatite (HA) powder (Plasma Biotal Limited, North Derbyshire, UK) was used in this study. Under the scanning electron microscope (SEM), the powder was needle-shaped with about 60 nm in diameter and 600 nm in length. The density of the powder was measured with a He pycnometer (AccuPyc 1330, Micromeritics Instrument Corp., Norcross, GA) to be 3.14 gm/cm^3. To assess the powder sinterability, cylindrical pellets of 12.7 mm in diameter and 4 mm in height were made by dry-pressing the HA powder at 34.5 MPa (5000 psi) in a stainless steel cylindrical die. These dry-pressed pellets were sintered in air at 800 °C, 900 °C, 1000 °C, 1100 °C, 1200 °C, 1300 °C and 1350 °C with a sintering rate of 10 °C/min. After sintering, the apparent density of each group was measured. The phase purity of the as-received powder and the sintered specimens were investigated with an X-ray diffractometer (XRD, Rotaflex, Rigaku, Tokyo, Japan). The samples were scanned from a 2 theta angle of 2° to 40° with a scanning speed of 2 /min. The as-received powder and the 1350 °C sample were also analyzed with a diffuse reflectance infra-red spectrophotometer (Galaxy 3020, Mattson Instrument Inc. Madison, WI) at a resolution of 4 cm^{-1} with wave number from 400 to 3000 cm^{-1}

2.2. Suspension preparation, curing and characterization

A mixture of 50 wt % propoxylated neopentoglycol diacrylate (PNPGDA) and 50 wt % isobornyl acrylate (IBA) was used as a suspension vehicle. To determine the optimal dispersant concentration, a 12 vol % HA/PNPGDA/IBA suspension was first prepared. A 1 : 1 mixture of quaternary ammonium acetate* and aromatic phosphate ester† was used as a dispersant for the ceramic powder. The dispersant was added to the 12 vol %

*Emcol CC-55, Witco Corp. Houston, TX.
†Emphos CS-1361, Witco Corp. Houston, TX.

HA/PNPGDA/IBA suspension at 1% to 6% to the dry ceramic powder weight. The viscosity of the suspension at each dispersant dose level was measured with a Bohlin Rheometer (Bohlin CS-50, Bohlin Instruments, Cranbury, NJ). The dispersant dose yielding the lowest viscosity was used for the rest of the study.

To investigate the effect of solids loading to the viscosity of the suspension, 5–40 vol % HA suspensions were prepared. This was done by incrementally adding the HA powder to the PNPGDA/IBA premix along with the experimentally determined dispersant dose, followed by vigorous mixing. The viscosity of the suspension at different solids loading was measured with a Bohlin Rheometer with a shear rate of between $0.01\,s^{-1}$ and $1000\,s^{-1}$.

A thermal curing mechanism was used to solidify the 40 vol % HA suspension, using Benzoyl Peroxide (BPO) at 0.15% to the monomer weight as a thermal initiator. The BPO decomposes upon heating, releasing free radicals that initiate the polymerization reaction of the PNPGDA/IBA monomers. A detailed analysis of acrylate curing is presented elsewhere [23]. To investigate the effect of the binders to the final phase purity of the ceramic, sintered samples prepared from the cured suspensions were analyzed with XRD. HA suspension was first cured in 14 ml glass vials at 85 °C for 1 h. The samples were removed from the glass vials and heated at a heating rate of 0.3 °C/min from room temperature to 550 °C to remove the acrylate binders. After binder removal, green bodies were sintered at 800 °C, 900 °C, 1000 °C, 1100 °C, 1200 °C, 1300 °C and 1350 °C. The phase purity of each specimen was again investigated by XRD. The amount of residual carbon in the 1350 °C specimen was analyzed with carbon coulometry at the Department of Geological Sciences at the University of Michigan. In carbon coulometry, a sintered HA specimen was combusted in a combustion apparatus and the amount of residual carbon was determined by the amount of CO_2 formed during combustion.

2.3. Implant design, manufacturing and characterization

Six tetragonal and cylindrical implants were designed. All implant designs are illustrated in Fig. 2a–d and the names and dimensions of these designs are summarized in Table I. The tetragonal prototype implants were designed with a commercial CAD software (Unigraphics V.11) on a Silicon Graphics Workstation. Square channels separated at equal distances were allowed to intersect vertically in X, Y, Z directions and penetrate throughout the tetragonal block. The cylindrical prototype implants were generated from an image manipulation process previously described [24]. In the cylindrical designs, C1 has channels intersecting in X, Y directions only and C2 has channels in all X, Y and Z directions. C3 design has a central column running in Z direction with channels extending from the center toward outside surface in radial directions. The negative images of the implant designs are shown in Fig. 2e–h to reveal the designed channel patterns inside the implants. These negative images were used to manufacture the molds on the Stereolithography apparatus with a commercial epoxy resin.*

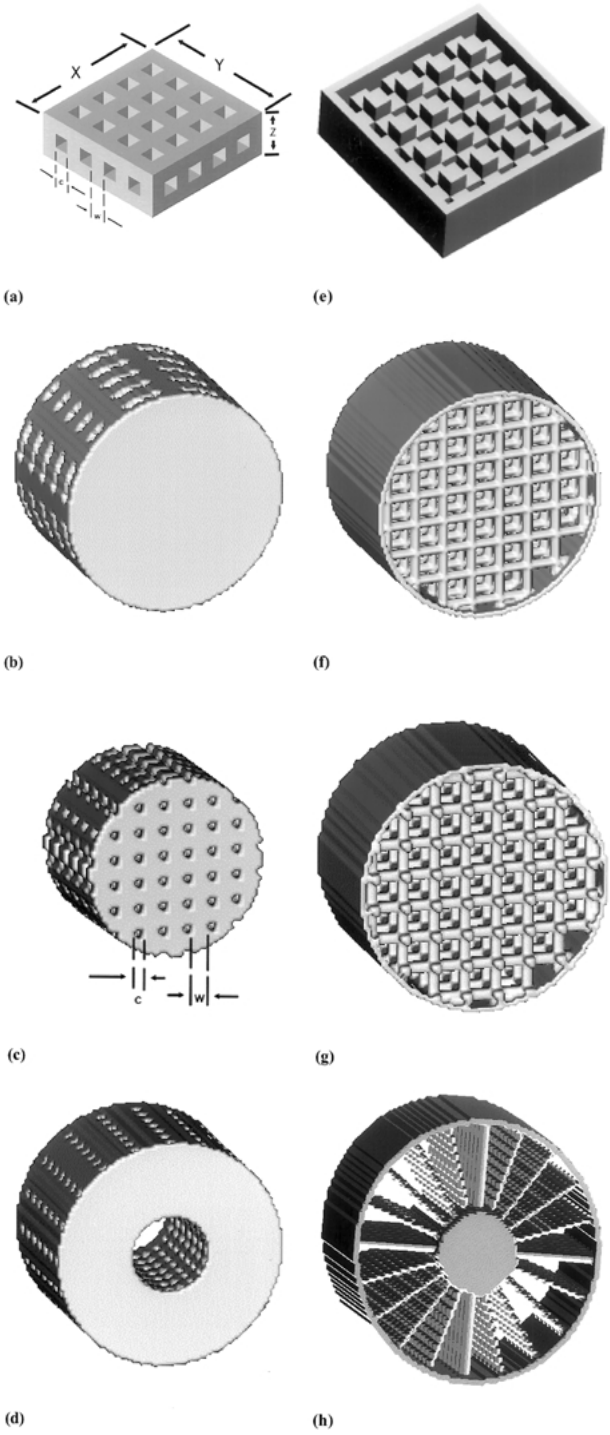

Figure 2 Implant designs (a) T1, T2 and T3 design, (b) C1 design, (c) C2 design, (d) C3 design, (e) negative image of T1, T2, T3 designs, (f)–(h) negative images of C1–C3 designs.

Before casting, the molds were cleaned with isopropanol alcohol. BPO initiator was mixed into the 40 vol % HA suspension just prior to casting. Vacuum was applied to the suspension to remove the entrapped air during suspension preparation. The 40 vol % HA/PNPGDA/IBA suspension was cast at room temperature

*Cibatool SL5170, 3D Systems, Valencia, CA.

TABLE I Dimensions of the implant designs

Design shape	Overall geometry	Channel size (c)	Wall size (w)
Tetragonal (T1)	$X, Y = 10.8$ mm $Z = 3.6$ mm	1200 μm	1200 μm
Tetragonal (T2)	$X, Y = 9.0$ mm $Z = 3.0$ mm	1000 μm	1000 μm
Tetragonal (T3)	$X, Y = 8.1$ mm $Z = 2.7$ mm	900 μm	900 μm
Cylindrical (C1)	Diameter = 8.25 mm Height = 10.90 mm	500 μm	800 μm
Cylindrical (C2)	Diameter = 9.49 mm Height = 6.01 mm	400 μm	800 μm
Cylindrical (C3)	Diameter = 9.51 mm Height = 6.51 mm	400 μm	

into the epoxy molds and cured at 85 °C for 1 h. The epoxy molds and the cured acrylic binders were pyrolyzed in an ashing furnace with a heating rate of 0.3 °C/min from room temperature to 550 °C. The green bodies were sintered at 1350 °C with a heating rate of 10 °C/min. Sintered HA implants were observed under optical and electron microscopes. The overall dimensions, channel size and wall size were measured under an optical microscope. The implant porosity was calculated from the weight and the overall volume of the implant. In this paper, ''implant porosity'' is used to describe the percentage of macroscopic void space in the implant resulting from the built-in channels. ''Sintering porosity'' is used to describe the percentage of microscopic voids left within the HA structure after the HA powder has gone through the sintering process.

3. Results

3.1. Powder characterization

Fig. 3 shows the sintered density versus temperature of the dry pressed pellet. The final density of the specimens sintered at 800 to 1350 °C was found to increase from 55% to 95% of the theoretical density. Sintered density of 95% occurred at 1290 to 1350 °C. The powder retained HA structure from room temperature up to 1350 °C without formation of any second phase detectable by XRD. The as-received powder was found to have IR peaks similar to the results described by Fowler [25]. The spectra shown in Fig. 4, had bands which were identified as followed: a ν_4PO_4 peak at 570 cm^{-1}, a smaller OH liberation peak at 650 cm^{-1}, a weak ν_1PO_4 peak at 960 cm^{-1}, and a strong ν_3PO_4 peak in the 1050 cm^{-1} to 1100 cm^{-1} region. A small peak for OH stretching was also) identified at 3600 cm^{-1}. In the 1350 °C sample, an additional peak was found in the 475 cm^{-1} region which was assigned a Ca_3-O stretching band [26].

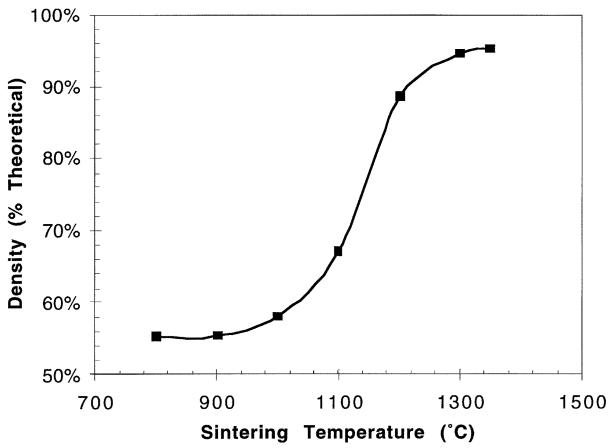

Figure 3 Sintering curve of HA powder from 800 °C to 1350 °C.

3.2. Suspension preparation and characterization

Fig. 5 shows the viscosity versus dispersant dose of the 12 vol % HA suspension. Without any dispersant added, the 12 vol % HA suspension was pasty. After 2% of the dispersant was added, the suspension was able to flow easily. At a dispersant dose of 3%, the suspension was shear-thinning. When the dispersant dose was increased to 4%, the 12 vol % suspension was apparently Newtonian with a constant viscosity of 0.45 Pa.S. The viscosity further decreased to 0.38 Pa.S at a dispersant dose of 4.7% and increased to 1.00 Pa.S again at a dose of

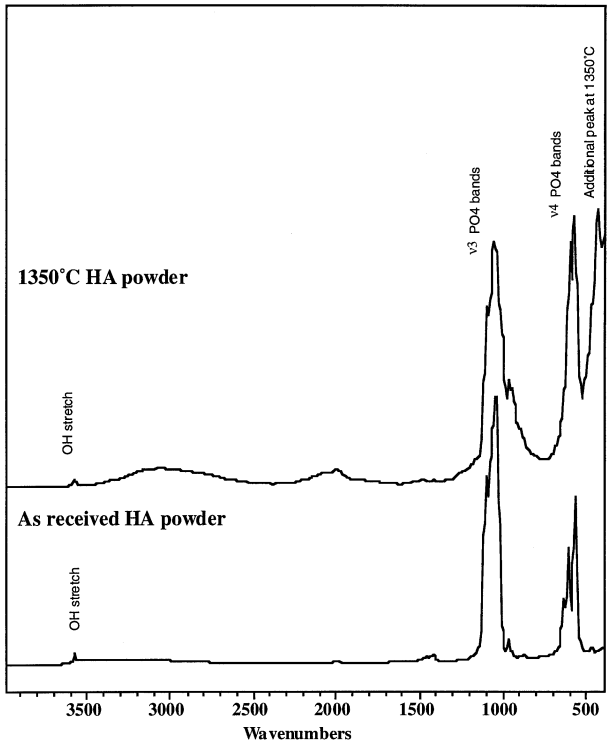

Figure 4 IR spectrum of as-received and 1350 °C powder. Extra peak was found at 475 cm^{-1} in the 1350 °C sample.

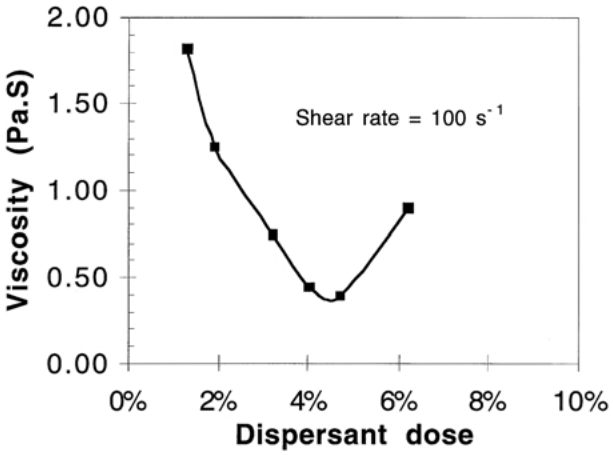

Figure 5 Viscosity of 12 vol% HA/PNPGDA/IBA suspension, with a 1 : 1 mixture of quarternary ammonium acetate and aromatic phosphate ester as the dispersant.

6%. A dispersant dose of 5% was used in preparing the 5–40 vol % HA suspension. Fig. 6 shows the measured viscosity versus the solids loading of the suspensions. The viscosity of the suspension was found to remain below 1 Pa.S at solid loadings lower than 30 vol %. The viscosity increased dramatically after 30 vol % and reached 15 Pa.S at a solid loading of 40 vol %. A detailed analysis of the rheological behavior is presented elsewhere [27].

With BPO added, the 40 vol % HA suspension cured into solid at 85 °C in less than an hour. After removing the epoxy mold and the acrylate binders, less than 0.5% of the residual carbon was found in the remaining HA green structure, as determined by carbon coulometer. Fig. 7 shows the XRD pattern of samples after sintering at 800 to 1350 °C. No second phase was detected in these sintered samples prepared from the cured suspensions. Fig. 8 shows the as-fired structure of the HA sample after sintering at 1350 °C for 1 h. The sintered HA microstructure was quite dense with $\sim 4\,\mu m$ equiaxial grains.

3.3. Implant design, manufacturing and characterization

The suspensions filled up the mold during casting without any difficulty. After curing at 85 °C for one hour, several cured specimens were sectioned and

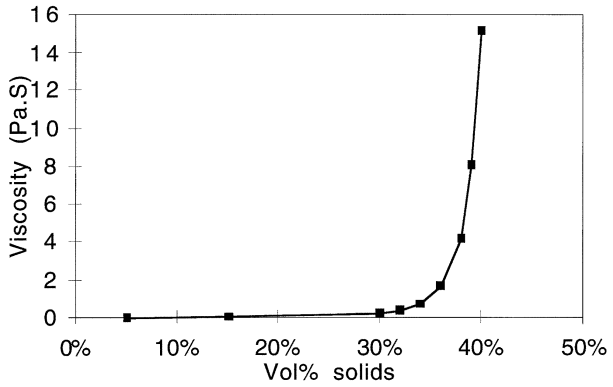

Figure 6 Viscosity of 5–40 vol % HA/PNPGDA/IBA suspension with 5% dispersant.

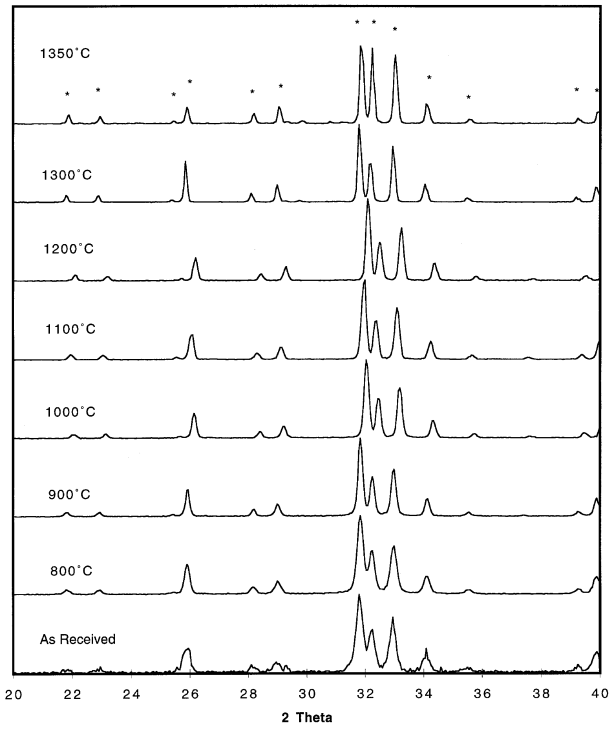

Figure 7 XRD pattern of as-received HA powder and specimens prepared from HA suspensions after curing at 85 °C and sintered at 800 °C to 1350 °C. * indicates HA peak.

examined. As shown in Fig. 9, no uncured suspension or empty voids were observed in the sectioned samples. After binder burnout and sintering, all of the HA implants came out successfully and were found to preserve the overall shape and designed channel patterns. Fig. 10 shows the sintered HA samples from all six designs. Several SEM pictures of the implants are shown in Fig. 11. Fig. 11 (a) shows the external surface of a C1 implant with top surface fractured to show the channels. Well-defined channel shape can be seen on the surface.

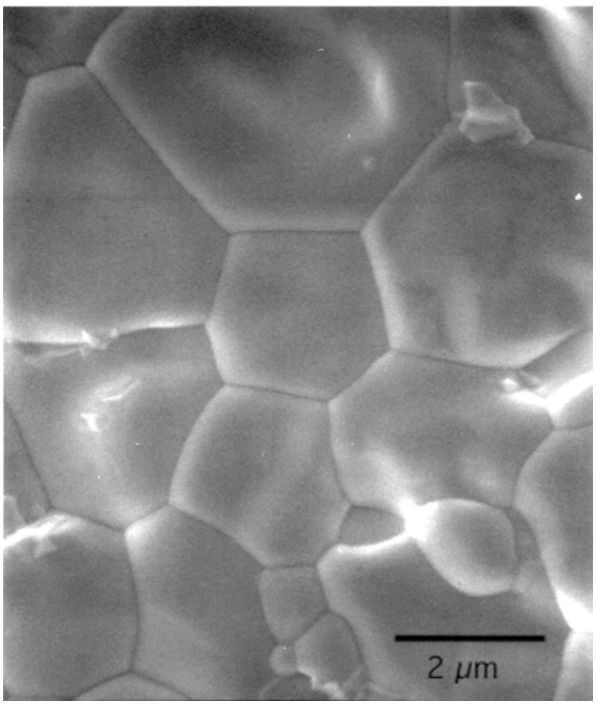

Figure 8 SEM micrograph of sintered HA showing densely sintered structure without open pores.

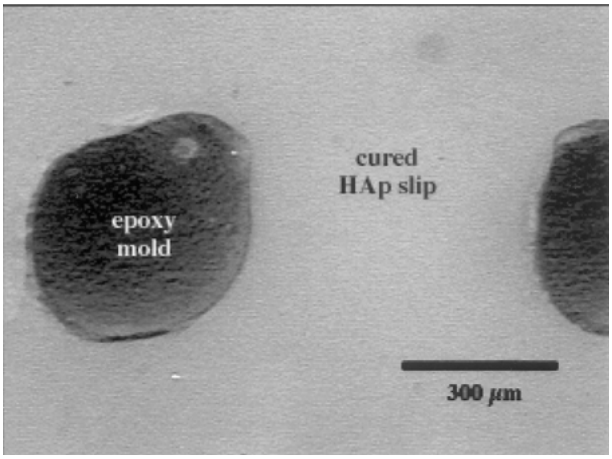

Figure 9 Cross-section of cured HA suspension inside the epoxy mold.

Fig. 11(b) shows the cross-section through the center column of a C3 implant, the center column to the left and the external surface to the right. Straight channels can be seen to connect the center column with the external surface. Fig. 11(c) shows the external surface of a C3 implant. The channels were found to exit the implant in a well-arranged pattern.

To check the uniformity of the sintering shrinkage, the dimensions of T1, T2, T3 and C1 were measured in several locations. The results are shown in Table II. The linear sintering shrinkage of these HA implants was found to fall in a small range between 25 and 27% with an average of $26 \pm 0.6\%$. The result indicates an even sintering shrinkage in the measured directions. Z direction in the tetragonal implants was not measures due to some material loss during sample polishing. To compensate for the shrinkage, the negative mold designs of C2 and C3 were expanded with a shrinkage factor of 1.37 before manufacturing on the SL apparatus. The molds were manufactured, cast and cured and the green bodies were sintered as previously described. Table III shows actual sintered diameter for C2 and C3. The difference between the design dimension and the sintered dimension reduced from 26% to 2% after the implementation of the shrinkage factor.

Table IV shows the range of channel size in all six designs. The average channel sizes in the tetragonal implants were between 693 and 968 μm. The average channel sizes in the cylindrical implants were between 366 and 444 μm. The later channel sizes are well in the range where most bone ingrowth was found [3, 9, 28, 29]. The standard deviations of the channel size in all designs are 50 μm or less. With different channel connection patterns, implant porosity between 26% and 52% was achieved.

4. Discussions

The sintering of Biotal HA powder has been studied by Ruys *et al*. [30]. The powder was found to exhibit a sigmoid sintering curve in the temperature-density data, with a plateau in the 1100 °C to 1350 °C range. The final sintered density was found to be between 81% and 99%. The shape of our temperature-density curve was similar to this research but with a plateau occurred at a higher temperature. The temperature for the plateau is known to

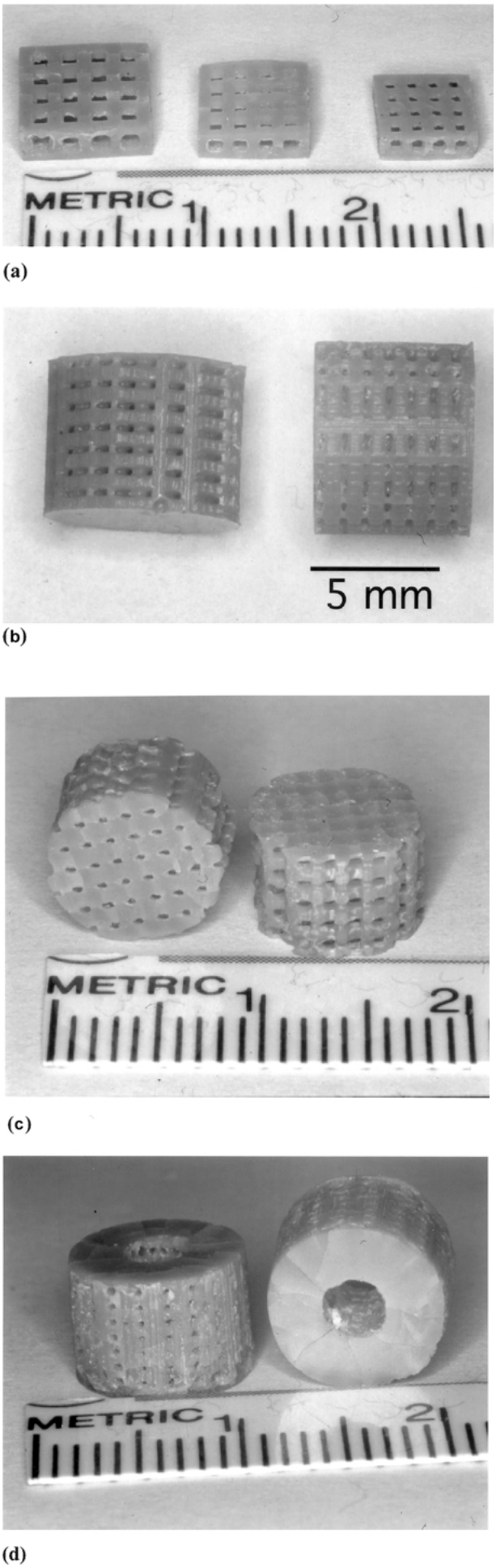

Figure 10 Sintered HA implants: (a) T1, T2, T3 design; (b) C1 design; (c) C2 design; (d) C3 design.

(d)

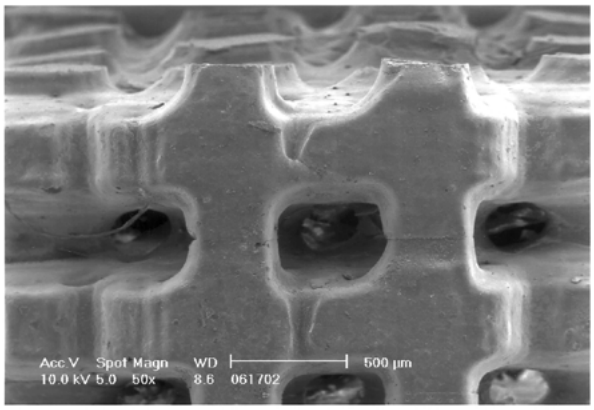

(a)

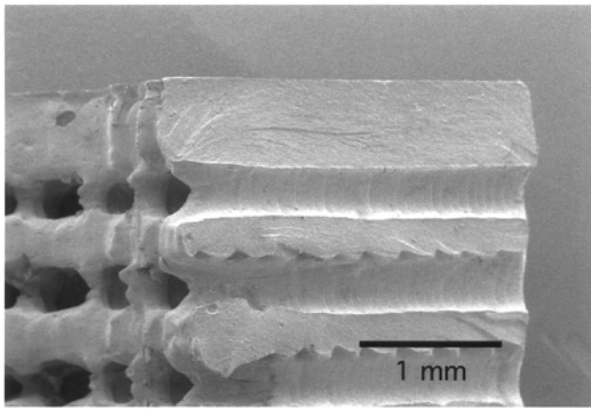

(b)

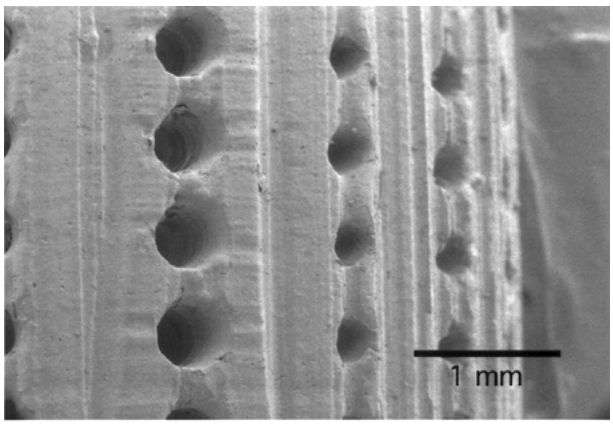

(c)

Figure 11 SEM pictures of sintered implants: (a) External surface of C1 implant with top surface fractured. The channel size and shape are well defined. (b) Vertically fractured C3 implant showing channels going from inside vertical column (left) to out side surface (right). (c) External surface of C3 implant showing well defined round channels.

be a function of particle size and shape and may vary from batch to batch [31].

It is known that that dehydroxylation in HA can occur without losing the HA structure when the mineral was heated at temperatures of 800 °C and above [32]. Elliott [26] has reviewed the IR spectrum study on the dehydroxylated HA, or oxyhydroxyapatite (OHA). The researcher concluded that the IR spectrum of OHA contains two additional principal peaks in the 500 to 400 cm^{-1} region (~ 475, $\sim 433\,cm^{-1}$) when compared with HA. The additional peak found in the 475 region was proposed to be a Ca_3-O stretching band resulted from the dehydroxylation. The 475 cm^{-1} extra peak in the IR result of our sintered specimen indicates an OHA formation in our final sintered implant. Ducheyne *et al*. found that OHA has an aqueous solubility between stoichiometric HA and β-Tricalcium phosphate (β-TCP) [33]. OHA is known to take up carbonate groups when submerged in simulated physiologic solutions [34]. The formation of carbonate-containing apatite on the surface of calcium phosphate ceramics may be an important step leading to bonding with bone [35].

In the process developed in this study, the molds were made by one of the most popular rapid prototyping techniques, StereoLithography [15]. The 40% HA suspension was found to fill up the 800 µm to 1200 µm space within the molds and solidified in a convenient curing time of 1 h at 85 °C. The organic binder was found to leave a small amount of residuals after binder burnout, which greatly reduced the possibility of adverse tissue response from the organic component of the suspension. The solid portions of the implant were composed of densely sintered hydroxyapatite which endow the implant with sufficient mechanical integrity to withstand future handling. The designed channel space and connection patterns were preserved during and after sintering. Since the 40 vol % HA suspension has a uniform sintering shrinkage of 26%, the shrinkage can be conveniently compensated by expanding the CAD design of the epoxy mold with appropriate shrinkage factor. As demonstrated in this investigation, the dimensional error between the designed value and the actual sintered implant was reduced to 2% by just one iteration.

The dimensional resolution of this process is of interest because it can determine the finest channel size achievable in the implant. In this study, the finest channel size achieved was about 366 µm. This, however, does not represent the lower limit of this process. The channels in the final HA implants are originally occupied by epoxy beams in the molds. The minimum size of the epoxy beams cured by the UV laser on SLA machine actually

TABLE II Final dimensions of T1, T2, T3 and C1 implants

Design	Measured value*(mm)	Sintering shrinkage (%)
Tetragonal (T1)	X, Y = 7.91 ± 0.13	26
Tetragonal (T2)	X, Y = 6.68 ± 0.06	25
Tetragonal (T3)	X, Y = 5.90 ± 0.02	27
Cylindrical (C1)	Diameter = 6.05 ± 0.02	26
Average		26 ± 0.6%

*Due to material lost in polishing, the *Z* dimensions were not measured.

TABLE III Final dimensions of C2 and C3 design. A shrinkage factor was introduced in the dimensions of the molds of these two designs

Design	Measured value* (mm)	Per cent error from original design
Cylindrical (C2)	Diameter = 9.26 ± 0.08	2
Cylindrical (C3)	Diameter = 9.31 ± 0.04	2

*Due to material lost in polishing, the Z dimensions were not measured.

TABLE IV Channel size, wall size and implant porosity of the sintered HA implants

Design shape	Channel size (μm)	Wall size (μm)	Implant porosity (%)
Tetragonal (T1)	968 ± 45	755 ± 48	52
Tetragonal (T2)	763 ± 50	693 ± 32	47
Tetragonal (T3)	693 ± 17	631 ± 37	48
Cylindrical (C1)	420 ± 24	560 ± 35	26
Cylindrical (C2)	444 ± 26	748 ± 17	44
Cylindrical (C3)	366 ± 36		38

determines the lower limit of the channels in the green state. Current He-Cd laser used on SLA250 has a laser spot size of 200 μm. This represents the lower limit of the cured epoxy beams in the mold, which is also the lower limit of the channel size in the implant in green state. An even smaller channel size can be expected after sintering. This lower limit in channel size will be utilized in future investigations. The range of implant porosity in this study was between 26% and 52%. We expect to create implants with a wider porosity range in subsequent studies.

We have successfully formulated a flowable 40 vol % HA suspension appropriate for casting. Epoxy molds designed with CAD software and CT scan images were made on an SLA machine. A HA suspension was successfully cast into the molds followed by binder burnout and sintering to yield HA implants with well-defined three-dimensionally interconnected channels. Hollister *et al*. [24] have successfully demonstrated the feasibility of using the combination of CT and CAD data to design implants with defined channel patterns. Porous HA with such characteristics can be a potential tool for studying the effect of channel size, channel connection pattern, and total porosity on cell ingrowth. The process developed in this study demonstrate that these porous HA implants with specific channel designs can actually be manufactured. The *in vivo* and *in vitro* studies of these implants are currently under investigation and will be reported in the future.

References

1. L. L. HENCH, *J. Am. Ceram. Soc.* **81** (1998) 1705.
2. E. SHORS and R. HOLMES, in ''An Introduction to Bioceramics'' edited by L. L. HENCH and J. WILSON (World Scientific, Singapore, 1993) p. 181.
3. M. EL DEEB and R. HOLMES, *J. Oral Maxillofac. Surg.* **47** (1989) 1282.
4. R. E. HOLMES, *Plast. Reconstruct. Surg.* **63** (1979) 626.
5. R. HOLMES, V. MOONEY, R. BUCHOLZ and A. TENCER, *Clin. Orthoped.* **188** (1983) 252.
6. C. A. VAN BLITTERSWIJK, J. J. GROTE, W. KUIJPERS, W. T. DAEMS and K. DE GROOT, *Biomaterials* **7** (1986) 137.
7. R. A. AYERS, S. J. SIMSKE, C. R. NUNES and L. M. WOLFORD, *J. Oral Maxillofac. Surg.* **56** (1998) 1297.
8. D. M. ROY and S. K. LINNEHAN, *Nature* **247** (1974) 220.
9. J.-H. KÜHNE, R. BARTL, B. FRISCH, C. HAMMER, V. JANSSON and M. ZIMMER, *Acta Orthop. Scand.* **65** (1994) 246.
10. U. RIPAMONTI, S. MA and A. REDDI, *Matrix* **12** (1992) 202.
11. D.-M. LIU, *Ceram. Int.* **23** (1997) 135.
12. *Idem., J. Mater. Sci. Lett.* **15** (1996) 419.
13. J. BOULER, M. TRECANT, J. DELECRIN, J. ROYER, N. PASSUTI and G. DACULSI, *J. Biomed. Mater. Res.* **32** (1996) 603.
14. E. TSURUGA, H. TAKITA, H. ITOH, Y. WAKISAKA and Y. KUBOKI, *J. Biochem.* **121** (1997) 317.
15. R. FEDCHENKO, in ''Stereolithography and other RP&M Technologies'', edited by P. Jacobs (ASME Press, Dearborn, MI, 1996) p. 2.
16. H. ANDERI, D. ZUR NEDDEN, W. MUHLBAUER, K. TWERDY, E. ZANON, K. WICKE and R. KNAPP, *Brit. J. Plast. Surg.* **47** (1994) 60.
17. T. BARKER, W. EARWAKER, N. FROST and G. WAKELEY, *Aust. Phys. Sci. Med.* **16** (1993) 79.
18. N. MANKOVICH, A. CHEESEMAN and N. STOKER, *J. Digital Imaging* **3** (1990) 200.
19. H. KLEIN, W. SCHNEIDER, G. ALZEN, E. VOY and R. GUNTHER, *Pediatr. Radiol.* **22** (1992) 458.
20. K. VENKATASWAMY, R. WAACK, B. NOVICH and J. HALLORAN, (1990) U.S. Patent 4,978,643.
21. M. A. JANNEY, (1990) U.S. Patent 4,894,194.
22. A. C. YOUNG, O. O. OMATETE, M. A. JANNEY and P. A. MENCHHOFER, *J. Am. Ceram. Soc.* **74** (1991) 612.
23. T.-M.G. CHU and J. HALLORAN, *J. Am. Ceram. Soc.* **83** (2000) 237.
24. S. HOLLISTER, T. M. CHU, R. E. GULDBERG, P. K. ZYSSET, R. A. LEVY, J. W. HALLORAN and S. E. FEINBERG, in ''IUTAM Synthesis in Biosolid Mechanics'', edited by P. PEDERSEN and M. BENDSOE (Kluwer Press, 1998) in press.
25. B. FOWLER, *Inorg. Chem.* **13** (1974) 194.
26. J. ELLIOTT, in ''Structure and Chemistry of the Apatites and Other Calcium Orthophosphates'', edited by J. ELLIOTT, (Elsevier, New York, 1994) p. 179.
27. T.-M.G. CHU and J. HALLORAN, *J. Am. Ceram. Soc.* **83** (2000) 2189.
28. G. DACULSI and N. PASSUTI, *Biomaterials* **11** (1990) 86.
29. O. GAUTHIER, J. BOULER, E. AGUADO, P. PILET, and G. DACULSI, *ibid.* **19** (1998) 133.
30. A. RUYS, M. WEI, C. SORRELL, M. DICKSON, A. BRANDWOOD and B. MILTHORPE, *ibid.* **16** (1995) 409.
31. A. RUYS, C. SORRELL, A. BRANDWOOD and B. MILTHORPE, *J. Mater. Sci. Lett.* **14** (1995) 744.
32. T. KIJIMA and M. TSUTSUMI, *J. Am. Ceram. Soc.* **62** (1979) 455.
33. P. DUCHEYNE, S. RADIN and L. KING, *J. Biomed. Mater. Res.* **27** (1993) 25.
34. S. R. RADIN and P. DUCHEYNE, *ibid.* **27** (1993) 35.
35. M. JARCHO, *Clin. Orthoped.* **157** (1981) 259.

Received 8 June
and accepted 14 December 1999